versity of Florida. Faculty in Chemistry at Georgia State University 1971–present. Approx. 150 publications. Research interests: biophysical analysis of nucleic acid structure and interactions with particular emphasis on the use of NMR information in conjunction with molecular modeling to understand drug action and to design new nucleic acid-interactive drugs.

Dynamic Angle Spinning

Philip J. Grandinetti
The Ohio State University, Columbus, OH, USA

1 INTRODUCTION

Dynamic angle spinning (DAS) is a two-dimensional NMR experiment designed for removing multiple-rank anisotropic broadenings in solid state NMR. It is a technique that has proven useful for obtaining the high-resolution isotropic solid state NMR spectra of the central transition of half-integer quadrupolar nuclei broadened to second order (see also ***Quadrupolar Nuclei in Solids***). This narrowing is accomplished by using the angle of the sample rotation axis as a dynamic variable in a two-dimensional experiment.

It has long been understood that the second-order anisotropic broadenings of the central transition of half-integer nuclei simply cannot be removed with magic angle or variable angle spinning,[1] and it was even thought that no spatial averaging solution existed. In 1988 new averaging approaches that solve this problem were disclosed by both the Pines group and the Virlet group at the 9th European Experimental NMR conference in Bad-Aussee. In subsequent publications by both groups[2,3] the underlying theory for removing second- and higher-order broadenings was presented, and two new experimental techniques emerged for removing second-order broadenings: double rotation (DOR) (see also ***Double Rotation*** and dynamic angle spinning (DAS), both first achieved experimentally at Berkeley.[2,4,5] DAS combines the ideas of switched rotation axis[6,7] and discrete averaging experiments[8] to remove the second-order broadenings of the central transition of half-integer nuclei.

In this article the basic principles behind DAS are discussed along with a description of how DAS is implemented and some illustrative examples of its use.

2 BASIC PRINCIPLES OF DYNAMIC ANGLE SPINNING

In NMR the Zeeman interaction is normally the dominant nuclear spin interaction, and the NMR transition frequency can be expanded in a perturbation series,[9]

$$\Omega(\theta,\phi) = \Omega^{(0)} + \Omega^{(1)}(\theta,\phi) + \Omega^{(2)}(\theta,\phi) + \cdots \quad (1)$$

with the Zeeman interaction as the zeroth-order term

$$\Omega^{(0)} = -\gamma B_0 \quad (2)$$

where γ is the nuclear gyromagnetic ratio and B_0 is the external magnetic field strength. The higher order terms in equation (1) are due to internal spin interactions (e.g. chemical shift, quadrupolar coupling, etc.). These interactions are second rank by nature and thus the higher order terms can be expanded in limited spherical harmonic series

$$\Omega^{(1)}(\theta,\phi) = \Omega^{(1)}_{\text{iso}} + \sum_{k=-2}^{2} c^{(1)}_{2,k} Y_{2,k}(\theta,\phi) \quad (3)$$

$$\Omega^{(2)}(\theta,\phi) = \Omega^{(2)}_{\text{iso}} + \sum_{k=-2}^{2} c^{(2)}_{2,k} Y_{2,k}(\theta,\phi) + \sum_{k=-4}^{4} c^{(2)}_{4,k} Y_{4,k}(\theta,\phi) \quad (4)$$

where (θ,ϕ) are the angles between the external magnetic field direction and the principal axis system of the internal spin interactions. The terms $\Omega_{\text{iso}}{}^{(n)}$ and the coefficients $c_{L,k}{}^{(n)}$ are listed in Tables 1 and 2 for the chemical shift and quadrupolar interactions.

In a liquid sample the random and rapid molecular reorientations average the NMR transition frequency over all values of θ and ϕ. This incoherent averaging over the full sphere removes all anisotropic broadenings and only the isotropic NMR frequencies are observed. This can be easily seen by averaging equations (3) and (4) over the sphere.

To obtain an isotropic spectrum from a solid sample, it is not necessary to average over all points on the entire sphere.[10] When the anisotropy in the NMR transition frequency is completely described by second-rank spherical harmonics, as in equation (3), the anisotropy can be coherently averaged away by reorientating the sample so that the external magnetic field is directed along only the three vertices on the face of an octahedron as shown in Figure 1(a). This is often the case with spin-$\frac{1}{2}$ nuclei. The discrete reorientation of the sample along these vertices is realized in a magic angle hopping (MAH)[8] experiment, (see also ***Magic Angle Turning & Hopping***) and the continuous rotation on a cone[10] with apex angle of 54.74° which passes through the vertices of the octahedron, is realized in a magic angle spinning (MAS)[11,12] experiment (see also ***Magic Angle Spinning***).

For list of General Abbreviations see end-papers

Table 1 Isotropic Frequency Shifts and Spherical Harmonic Coefficients for the $m \rightarrow m-1$ Transition of Spin I from First-Order Perturbation Theory for Chemical Shift and Quadrupolar Interactions[a]

	Chemical shift	Quadrupolar
$\Omega_{iso}^{(1)}$	$\sigma\gamma B_0$	0
$c_{2,0}^{(1)}$	$\sqrt{\frac{4\pi}{5}} \cdot \gamma B_0(\sigma_{ZZ} - \sigma)$	$\sqrt{\frac{9}{5}} \cdot \frac{\pi^{3/2}\chi}{I(2I-1)}(2m-1)$
$c_{2,\pm2}^{(1)}$	$\sqrt{\frac{2\pi}{15}} \cdot \gamma B_0(\sigma_{YY} - \sigma_{XX})$	$\sqrt{\frac{3}{10}} \cdot \frac{\pi^{3/2}\chi\eta}{I(2I-1)}(2m-1)$

[a] σ_{XX}, σ_{YY}, σ_{ZZ} are the principal components of the chemical shift tensor, χ is e^2qQ/h, and η is the quadrupolar asymmetry parameter.

For NMR transition frequencies with higher than first-order terms, octahedral symmetry may not be sufficient for obtaining an isotropic spectrum. For example, if the quadrupolar coupling is sufficiently large that the second-order term is required to describe the spectrum, then the size of the first-order broadening can be on the order of many MHz; thus it can be virtually impossible to obtain the complete NMR spectrum of a quadrupolar nucleus in a polycrystalline sample, since the bandwidth of conventional NMR spectrometers is typically only a few hundred kHz. Fortunately, for half-integer spin quadrupolar nuclei, the central $m = \frac{1}{2} \rightarrow -\frac{1}{2}$ transition is unaffected by the first-order quadrupolar term and in many cases is broadened only by the second-order term of equation (4), which can be on the order of a few kHz. Unfortunately, while the second-rank spherical harmonics in equation (4) are removed using octahedral symmetry, the fourth-rank spherical harmonics are not. Therefore, to average away completely the anisotropy in this case a better approximation to the sphere is required. This can be done by reorientating the sample so that the external magnetic field is directed along the six vertices on the icosahedron as shown in Figure 1(b) or in Figure 1(c). The discrete reorientation of the sample along these vertices is realized in a dynamic angle hopping (DAH)[13] experiment and the continuous rotation on two cones[10] with apex angles of 0° and 63.43° or 37.38° and 79.19°,

Table 2 Isotropic Frequency Shifts and Spherical Harmonic Coefficients for the $m \rightarrow m-1$ Transition of Spin I from Second-order Perturbation Theory for the Quadrupolar Interaction[a]

$\Omega_{iso}^{(2)}$	$-\frac{3}{10}\frac{\pi^2\chi^2}{I^2(2I-1)^2\gamma B_0}\left(\frac{\eta^2}{3}+1\right)[I(I+1)-9m(m-1)-3]$
$c_{2,0}^{(2)}$	$\sqrt{\frac{36}{245}}\frac{\pi^{5/2}\chi^2}{I^2(2I-1)^2\gamma B_0}\left(\frac{\eta^2}{3}-1\right)[2I(I+1)-9m(m-1)-15/4]$
$c_{2,\pm2}^{(2)}$	$\sqrt{\frac{24}{245}}\frac{\pi^{5/2}\chi^2\eta}{I^2(2I-1)^2\gamma B_0}[2I(I+1)-9m(m-1)-15/4]$
$c_{4,0}^{(2)}$	$\frac{3}{35}\frac{\pi^{5/2}\chi^2}{I^2(2I-1)^2\gamma B_0}\left(\frac{\eta^2}{18}+1\right)[9I(I+1)-51m(m-1)-39/2]$
$c_{4,\pm2}^{(2)}$	$\frac{1}{\sqrt{490}}\frac{\pi^{5/2}\chi^2\eta}{I^2(2I-1)^2\gamma B_0}[9I(I+1)-51m(m-1)-39/2]$
$c_{4,\pm4}^{(2)}$	$\frac{1}{\sqrt{1260}}\frac{\pi^{5/2}\chi^2\eta^2}{I^2(2I-1)^2\gamma B_0}[9I(I+1)-51m(m-1)-39/2]$

[a] χ is e^2qQ/h and π is the quadrupolar asymmetry parameter.

For References see p. 1776

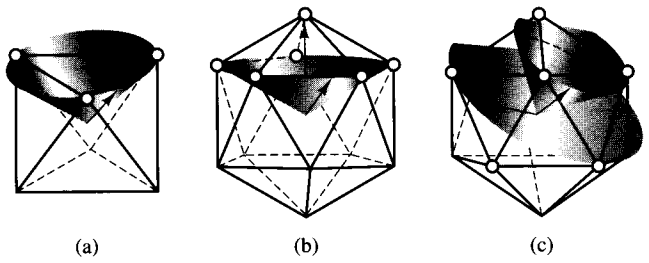

Figure 1 (a) Octahedral symmetry can be implemented with a single continuous trajectory in cases where tensors of rank 2 are to be eliminated. (b,c) Icosahedral symmetry can be implemented with just two continuous trajectories in cases where tensors of rank 2 and 4 are to be eliminated. Time spent along one particular trajectory is proportional to the number of vertices. In (b) the two spinning axes are $\beta_1 = 0°$ and $\beta_2 = 63.43°$, and the ratio of times spinning at the two angles is 1:5. In (c) the angles are $\beta_1 = 37.38°$ and $\beta_2 = 79.19°$, and the ratio of times spinning at the two angles is 1:1. (Adapted by permission of Elsevier Science Publishers from B. Q. Sun, J. H. Baltisberger, Y. Wu, A. Samoson, and A. Pines, 'Solid State NMR', 1992, **1**, 267, and by permission of Clarendon Press from Samoson et al.)

which pass through the icosahedral vertices, is realized in a dynamic angle spinning (DAS)[3–5,10,14–21] experiment.

A DAS reorientation trajectory is implemented as a two-dimensional NMR experiment which correlates a spin's resonance frequency while spinning at one angle with its frequency while spinning at a second angle. In DAS the sample is spun about a single axis for the first evolution period and then hopped to a second angle for the second evolution period as shown in Figure 2(a). Two rf pulses are used to quench the evolution during the time required to hop.

When spinning about a single axis equations (3) and (4) are averaged to

$$\overline{\Omega^{(1)}}(\beta,\theta',\phi') = \Omega_{\text{iso}}^{(1)} + P_2(\cos\beta)\sum_{m=-2}^{2} c_{2,m}^{(1)} Y_{2,m}(\theta',\phi') \tag{5}$$

$$\overline{\Omega^{(2)}}(\beta,\theta',\phi') = \Omega_{\text{iso}}^{(2)} + P_2(\cos\beta)\sum_{m=-2}^{2} c_{2,m}^{(2)} Y_{2,m}(\theta',\phi') + P_4(\cos\beta)\sum_{m=-4}^{4} c_{4,m}^{(2)} Y_{4,m}(\theta',\phi') \tag{6}$$

where β is the angle between the spinner axis and the magnetic field, $P_n(\cos\theta)$ are Legendre polynomials, and (θ',ϕ') are the angles between the spinner axis and the principal axis system of the internal spin interactions. If the two rotor axis angles in a DAS experiment are chosen so that for all the spins the anisotropic frequency at the first angle is mirrored about the isotropic frequency when spinning at the second angle, then all decay of the signal in t_1 due to the anisotropic broadening is refocused into an echo during t_2. For systems broadened up to second order this mirror image condition is fulfilled when the angle pair (β_1,β_2) satisfies the conditions

$$x_1 P_2(\cos\beta_1) + x_2 P_2(\cos\beta_2) = 0 \tag{7}$$

$$x_1 P_4(\cos\beta_1) + x_2 P_4(\cos\beta_2) = 0 \tag{8}$$

For list of General Abbreviations see end-papers

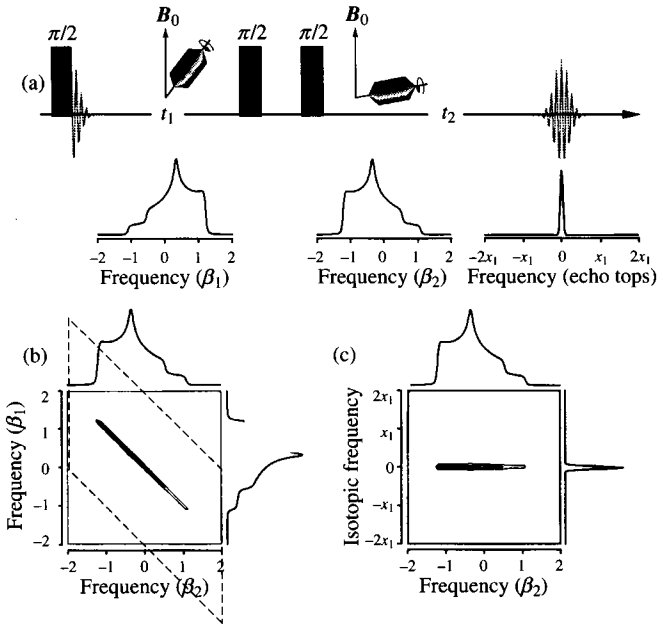

Figure 2 (a) Simplest implementation of 2D DAS pulse sequence. (b) 2D variable angle spinning correlation spectrum obtained from the sequence in (a). (c) 2D DAS spectrum obtained from (b) after applying the shearing transformation as described in the text

and

$$x_1 + x_2 = 1 \tag{9}$$

The DAS echo forms at a time $(x_2/x_1)t_1$ during t_2 evolution. By collecting the intensity of the echo tops as a function of t_1/x_1 and Fourier transforming this interferogram, the isotropic DAS spectrum is obtained. By collecting all the data in t_2 as a function of t_1, and performing a 2D Fourier transform, a spectrum as shown in Figure 2(b) is obtained. This 2D spectrum correlates the NMR spectrum obtained while spinning at β_1 with the NMR spectrum obtained while spinning at β_2. If the angle pair (β_1,β_2) satisfies equations (7)–(9), then the 2D correlation for each site will be isotropic and linear and given by:

$$\omega_2 = \frac{1}{x_2}(\Omega_{\text{iso}} - x_1\omega_1) \tag{10}$$

There is a continuous set of angle pairs that exist which provide this isotropic 2D correlation, including the angle pairs (0°,63.43°) where $x_1/x_2 = 5$ and (37.38°, 79.19°) where $x_1/x_2 = 1$. Equations (7)–(9) may be solved analytically for the angle pairs (β_1,β_2) in terms of x_1 and x_2:

$$\beta_1 = \cos^{-1}\frac{\sqrt{1+\sqrt{\frac{4x_2}{5x_1}}}}{3} \tag{11}$$

$$\beta_2 = \cos^{-1}\frac{\sqrt{1-\sqrt{\frac{4x_1}{5x_2}}}}{3} \tag{12}$$

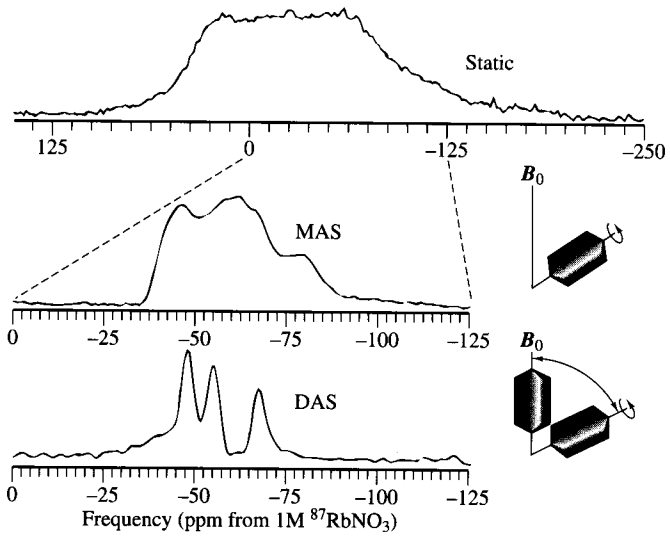

Figure 3 Static, MAS, and DAS ^{87}Rb NMR spectra of polycrystalline $RbNO_3$

where $0.8 \leqslant x_2/x_1 \leqslant 5$. Of course, the order of the angle pair may be reversed with a corresponding reversal of the fractional time spent at each angle.

The 2D spectrum of Figure 2(b) can be transformed with a shearing transformation to obtain the 2D DAS spectrum shown in Figure 2(c), which correlates the isotropic resonance of a site with its anisotropic lineshape. Shearing transformations are well known in NMR.[22] In DAS the 2D spectrum is sheared by an angle θ_S, given by

$$\theta_S = \tan^{-1}\left(\frac{x_2}{x_1}\right) \tag{13}$$

followed by a scaling of the ω_1 axis by x_1. The shearing transformation may be implemented by applying a t_1-dependent first-order phase correction:

$$S'(t'_1, \omega'_2) = e^{i\phi(t_1,\omega_2)} S(t_1, \omega_2) \tag{14}$$

where

$$\phi(t_1, \omega_2) = \left(\frac{x_2}{x_1}\right)\omega_2 t_1 \tag{15}$$

before the final Fourier transform with respect to t'_1. This correction removes the tilting in $S(\omega_1,\omega_2)$, transforming it into $S'(\omega'_1,\omega'_2)$, so that an isotropic spectrum may be obtained from a projection onto the ω'_1 axis.

Figure 3 depicts the static, MAS, and DAS spectra of polycrystalline $RbNO_3$. $RbNO_3$ contains three inequivalent Rb sites in its unit cell. While the MAS provides considerable narrowing of the static spectrum by removing the second-rank spherical harmonic orientational broadenings, it still contains scaled fourth-rank orientational broadenings. With DAS, both second- and fourth-rank orientational broadenings are removed and the three inequivalent Rb sites can be resolved.

Because DAS is a two-dimensional experiment it is more time consuming than MAS; however, DAS does provide a means of separating the anisotropic lineshapes correlated to the isotropic frequency of each resolved site. For example, Figure 4 depicts the 2D DAS spectrum of $RbNO_3$. Since the isotropic resonances of all three inequivalent Rb sites can be resolved, cross sections correlated to each isotropic frequency provide the separated anisotropic lineshape for each site. These separated lineshapes can be analyzed to obtain the quadrupolar coupling parameters associated with each resonance. This information can be useful in providing structural information. For example, in the case of $RbNO_3$, a simple point charge calculation of the electric field gradients at each Rb site in the unit cell gives quadrupolar asymmetry parameters of approximately 0.9, 0.6, and 0.3. On this basis, the three resonances in the 2D DAS spectrum can be assigned to the three sites in the unit cell as shown in Figure 4. This approach can also be extended to amorphous solids where a continuous set of overlapping anisotropic lineshapes can also be separated according to correlated isotropic frequencies and used to quantify continuous structural distributions.

An interesting consequence of the shearing transformation in DAS is that the spinning sidebands can appear at nonintegral multiples of the spinning speed in the isotropic dimension. A

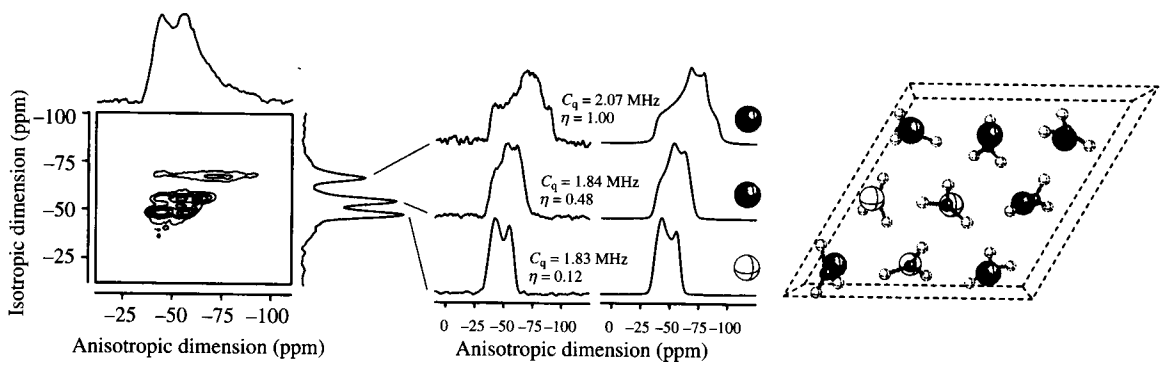

Figure 4 On the left is the two-dimensional ^{87}Rb DAS NMR spectrum of $RbNO_3$ at 4.2 T. Cross sections from this spectrum provide the separated one-dimensional anisotropic lineshapes for each ^{87}Rb site. These lineshapes can be fitted to obtain the quadrupolar coupling parameters for each site. In this case each resonance could be assigned to a Rb site in the unit cell (shown on the right) by comparing the electric field gradients obtained from the measured quadrupolar coupling constants with the electric field gradient at each Rb site obtained from a simple point charge model calculation (see text). (Adapted by permission of Academic Press from Grandinetti et al.[20]

For References see p. 1776

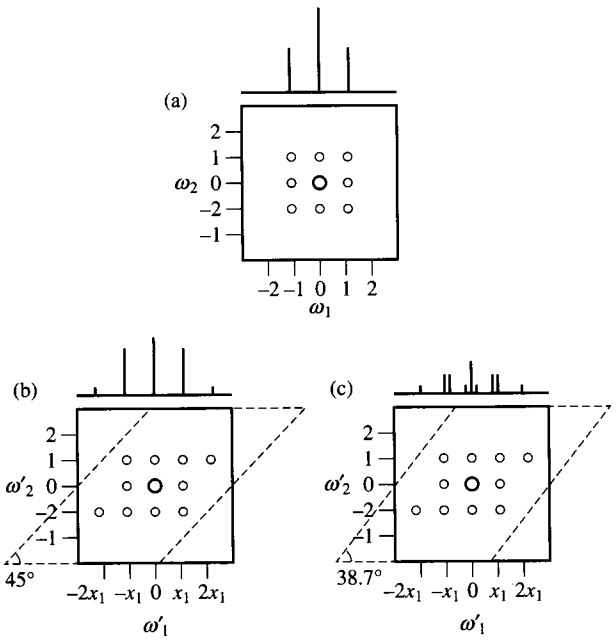

Figure 5 Schematic examples of the effects of the shearing transformation on sideband positions in DAS. (a) Unsheared 2D spectrum. (b) Sheared 2D spectrum obtained from the two-dimensional spectrum in (a) by a shearing transformation employing a shearing angle of 45° and a scaling of the ω_1 by $x_1 = 0.5$. In this case the spinning sidebands in the 2D spectrum are aligned with respect to ω'_1 so that a projection onto the ω'_1 axis only contains spinning sidebands separated by integer multiples of $0.5\Omega_R$. (c) Sheared 2D spectrum obtained from the 2D spectrum in (a) by a shearing transformation employing a shearing angle of 38.7° and a scaling of the ω_1 by $x_1 = 0.56$. In this case the spinning sidebands in the 2D spectrum are not aligned with respect to ω'_1 so that a projection onto the ω'_1 axis contains spinning sidebands that are separated by multiples of and also sum and difference frequencies of $x_1\Omega_R = 0.56\Omega_R$ and $x_2\Omega_R = 0.44\Omega_R$. (Reproduced by permission of Academic Press from P. J. Grandinetti, Y. K. Lee, J. H. Baltisberger, B. Q. Sun, and A. Pines, *J. Magn. Reson.*, 1993, **102**, 71)

schematic example of the behavior of spinning sidebands after a shearing transformation is shown in Figure 5 for the two cases $\theta_s = 45°$ and $\theta_s = 38.7°$. The frequency axes in Figure 5(a) are in units of Ω_R, the actual spinning speed. The example in Figure 5(b) is the familiar situation in 2D echo spectroscopy, where the dephasing and refocusing times are equal (e.g. 2D *J* spectroscopy). In this example even though the spectrum is sheared, the sidebands remain aligned such that a projection onto the ω'_1 axis contains only sidebands at integer multiples of $0.5\Omega_R$. In contrast, the example in Figure 5(c), where $x_1 = 0.44$ and $x_2 = 0.56$, describes a 2D echo experiment with unequal dephasing and refocusing times. In this situation the spinning sidebands are not aligned in ω'_1, and consequently a projection onto ω'_1 yields a fairly complicated sideband pattern.

Simulated and experimental isotropic projections from the ^{87}Rb DAS of $RbClO_4$, demonstrating the sideband behavior for various pairs of DAS angles, are shown in Figure 6. In each isotropic 1D DAS spectrum the spinning sidebands appear at integral multiples of $x_1\Omega_R$ and $x_2\Omega_R$ and also at the sum and difference frequencies of the integral multiples of $x_1\Omega_R$ and

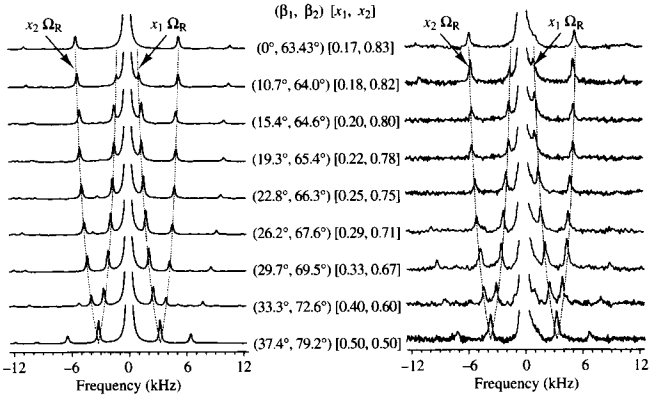

Figure 6 Simulated and experimental 1D DAS spectra of $^{87}RbClO_4$ for various rotor angle pairs (β_1,β_2) and fractions $[x_1,x_2]$. All spectra were obtained with a rotor frequency of $\Omega_R = 6.4$ kHz. The quadrupolar coupling parameters of $RbClO_4$ used in the simulations are $C_q = 3.2$ MHz and $\eta = 0.1$. (Adapted by permission of Academic Press from P. J. Grandinetti, Y. K. Lee, J. H. Baltisberger, B. Q. Sun, and A. Pines, *J. Magn. Reson.*, 1993, **102**, 71)

$x_2\Omega_R$. The angle pair (37.78°, 79.19°) has an advantage that $x_1\Omega_R = x_2\Omega_R = 0.5\Omega_R$ and a simple sideband spacing of $0.5\Omega_R$ is obtained. Of particular interest is the fact that the 1D DAS spectrum for the (0°,63.43°) angle pair contains only spinning sidebands at multiples of $x_2\Omega_R = 0.83\Omega_R$. The spinning sidebands at $x_1\Omega_R = 0.17\Omega_R$ do not exist and thus the (0°,63.43°) angle pair provides the highest effective spinning speed when removing first- and second-order broadenings with DAS.

The (0°,63.43°) angle pair offers other advantages, in particular for cross polarization (CP) experiments (see also ***Cross Polarization in Rotating Solids: Spin-1/2 Nuclei***). Vega[23,24]

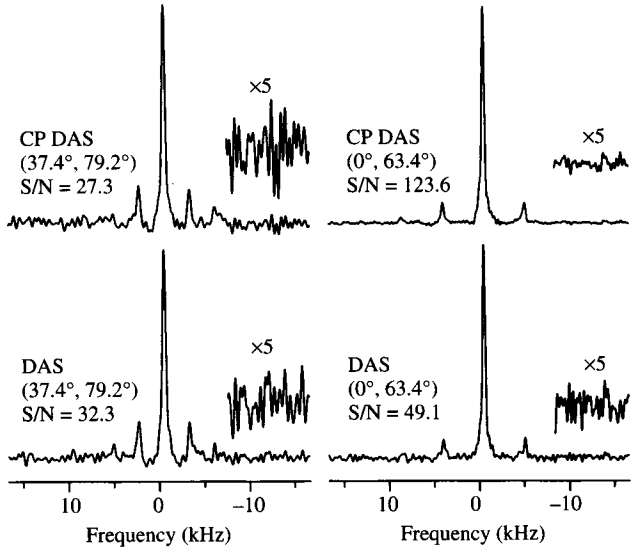

Figure 7 DAS and CP DAS spectra of sodium pyruvate acquired using the DAS angle pairs (37.38°,79.19°) and (0°,63.43°). With (0°,63.43°) an improvement of 2.5 in S/N ratio is observed with CP compared with the spectrum taken without CP. In addition, the CP DAS experiment using (0°,63.43°) has an S/N ratio over 4.5-times that of the CP DAS experiment using (37.38°,79.19°). (Reproduced by permission of Taylor & Francis Ltd. from Baltisberger et al.[25])

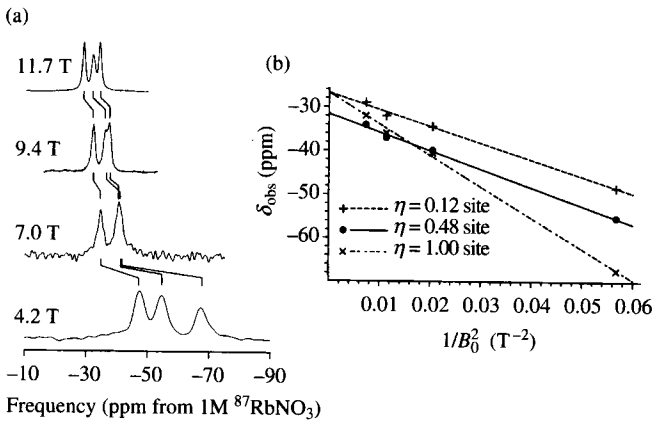

Figure 8 (a) ^{87}Rb DAS spectra of $RbNO_3$ collected at (a) 11.7 T, 9.4 T, 7.0 T, and 4.2 T. (b) Isotropic shifts of $^{87}RbNO_3$ plotted versus $1/B_0^2$ and fitted using a linear least-squares routine. The intercepts and slopes are used to calculate the values of $\delta_{iso}^{(CS)}$ (ppm) and $C_q(1 + \eta^2/3)^{\frac{1}{2}}$ (MHz), respectively. (Reproduced by permission of Academic Press from Baltisberger et al.[16])

has shown that it may be difficult or even impossible to obtain efficient CP transfer of all sites in a multisite system when spinning at the magic angle. This problem can be eliminated in a DAS experiment by exploiting the time independence of the spin eigenvalues when spinning at 0° (parallel) to the external magnetic field. By performing the CP step while spinning at 0° the full static CP intensity can be recovered.[25] In Figure 7, the decoupled DAS and CP DAS spectra of sodium pyruvate for the (37.38°,79.19°) and (0°,63.43°) angle pairs illustrate the significant increases in signal-to-noise ratio (S/N) that can be obtained with the (0°,63.43°) angle pair.

From Tables 1 and 2 it is clear that the isotropic frequency shifts of both the first-order chemical shift and the second-order quadrupolar shift have different dependences on the external magnetic field strength. These different dependences can be exploited as a means of separating the isotropic chemical and quadrupolar shifts. In Figure 8(a) the isotropic ^{87}Rb DAS spectra of $RbNO_3$ measured at four different magnetic fields are depicted. As shown in Figure 8(b), the isotropic resonance frequency in ppm for each site is a linear function of $1/B_0^2$ with the isotropic chemical shift given by the intercept and the second-order quadrupolar shift given by the slope.[16]

3 IMPLEMENTATION OF DYNAMIC ANGLE SPINNING

Four variants of the DAS pulse sequence are depicted in Figure 9. The simplest implementation is shown in Figure 9(a). In this sequence, DAS can be viewed as a 2D exchange experiment with a rotor reorientation during the mixing time and, as in the 2D exchange experiment, an amplitude-modulated response in t_1 makes it possible to obtain pure-absorption-mode 2D spectra using the hypercomplex or TPPI (time proportional phase increment) approach to 2D data acquisition. The hypercomplex data acquired with this sequence are Fourier-transformed and phase-corrected in a manner similar to that described elsewhere,[22] with the only difference being the shearing transformation described by equations (14) and (15).

In Figure 9(b), a different approach is taken that provides pure absorption-mode lineshapes in addition to a $\sqrt{2}$ increase in the signal-to-noise ratio. In this approach, the coherence-transfer echoes, which are formed because of the inhomogeneous broadenings intrinsic to the DAS experiment, are time-shifted by an amount τ with a π pulse to obtain whole echo acquisition in t_2, and thus a pure absorption mode 2D spectrum. The length of τ is a multiple of the rotor period, and typically large enough so that the echo in t_2 begins at zero. Only the $p = 0 \rightarrow -1 \rightarrow 0 \rightarrow 1 \rightarrow -1$ pathway is selected in this case. The complex 2D data acquired with this sequence are processed in the same fashion as conventional phase-modulated 2D data, with the only difference being a τ-dependent first-order phase correction of

$$\phi(\tau, \omega) = \omega_2 \tau \tag{16}$$

to remove the phase modulation because of the time-shifted echo, in addition to the shearing transformation described by equations (14) and (15). When there is an inhomogeneous broadening associated with the isotropic DAS dimension, both pathways shown in Figure 9(b) can be acquired using the hypercomplex approach for an additional $\sqrt{2}$ increase in signal-to-noise ratio. This often occurs when DAS is applied to

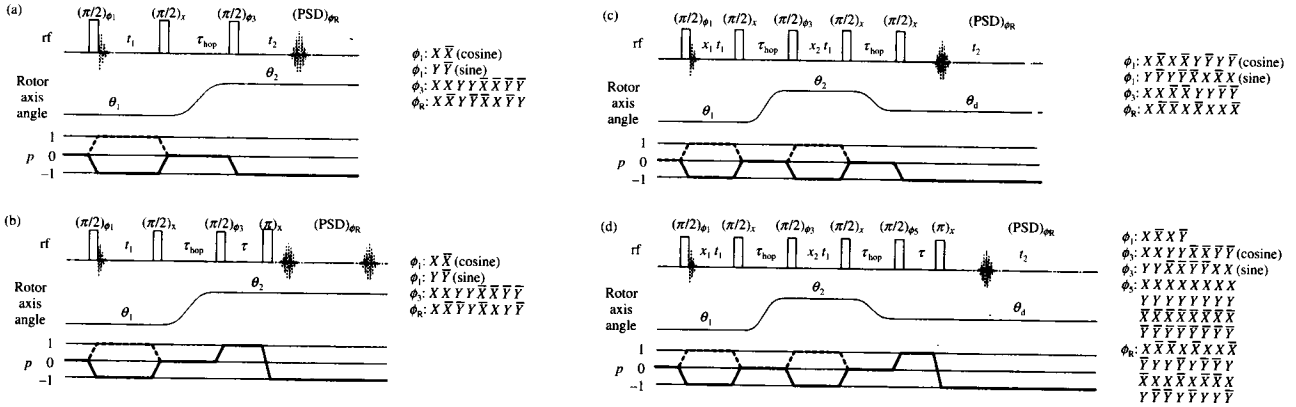

Figure 9 Pulse sequences, coherence transfer pathways, and minimal phase cycles for (a) dynamic angle spinning, (b) shifted echo dynamic angle spinning, (c) MAS-detected dynamic angle spinning, and (d) MAS-detected shifted echo dynamic angle spinning

For References see p. 1776

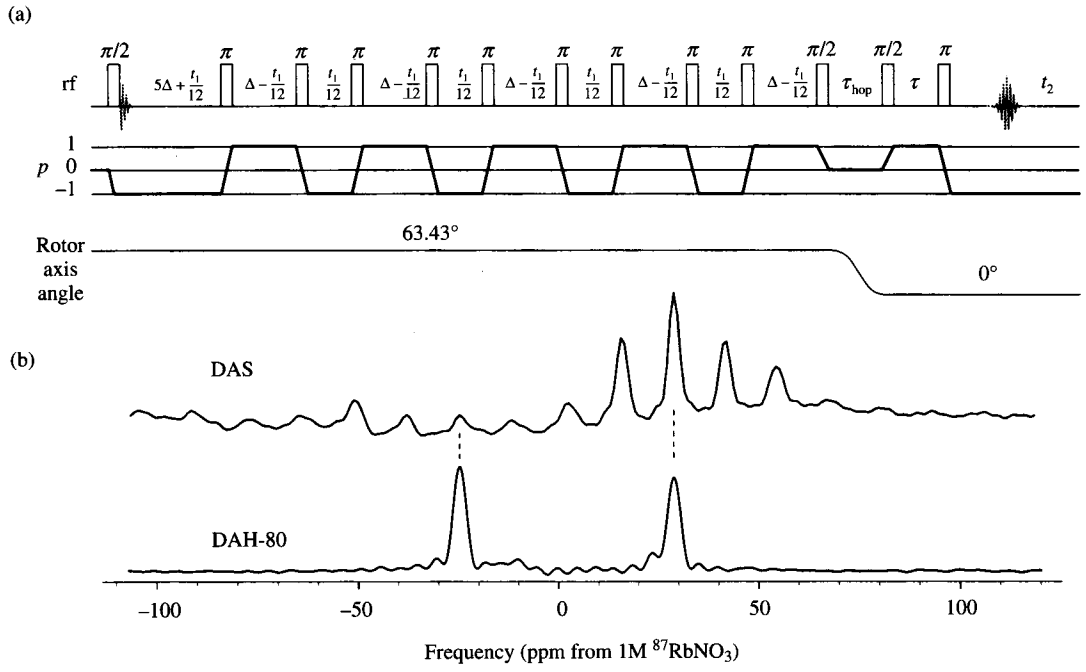

Figure 10 (a) DAH-180 pulse sequence which produces sideband-free dynamic angle spinning spectra. The experiment is performed over N rotor cycles with a rotor period of τ_r. $\Delta = N\tau_r/10$. (b) Comparison of the ^{87}Rb spectra of Rb_2SO_4 taken at 9.4 T at a spinning frequency of 1.8 kHz using DAS (with side bands) and using DAH-180 (sideband-free). (Reproduced by permission of Elsevier Science Publishers from Gann et al.[13])

materials in which there is a continuous distribution of atomic environments resulting in a continuous distribution of second-order quadrupolar and isotropic chemical shifts.

Mueller et al.[18] pointed out that extracting the quadrupolar coupling parameters from the anisotropic DAS dimension can be difficult when additional chemical and dipolar anisotropies are present. Chemical shift and dipolar anisotropic broadenings can be removed when spinning at 54.74°, leaving only quadrupolar anisotropic broadening; 54.74°, unfortunately, is not a solution of equations (11) and (12). The solution of Mueller et al.[18] was to incorporate a second rotor reorientation into the DAS sequence so that the final angle for detection is the magic angle. This approach and its shifted echo variant are shown in Figure 9(c) and Figure 9(d). With the evolution times defined in Figure 9(c) and Figure 9(d) a shearing transformation is not necessary to obtain the isotropic/anisotropic 2D DAS spectrum; however, for the shifted echo experiment the phase correction of equation (16) is still required.

Using rotor-synchronized π pulses it is possible to eliminate all sidebands in a DAS experiment using the DAH-180 sequence of Gann et al.,[13] shown in Figure 10. Under this pulse sequence all evolution at 63.43° that does not contribute to t_1 evolution is refocused by spending equal time as +1 and −1 coherences, while all t_1 evolution occurs only as −1 coherences. This sequence has the advantage that the intensities of the suppressed sidebands are completely transferred to the centerband, unlike other sideband suppression techniques such as TOSS.[26] In contrast to the DAS sequences in Figure 9, the DAH-180 sequence has a trade-off between sensitivity and resolution. DAH-180 is a constant time experiment, so in order to increase the resolution a larger constant time is required which then leads to increased intensity losses via T_2 relaxation processes.

There are a few limitations of the DAS technique, most notably being its current inability to refocus homonuclear dipolar broadenings. This is a consequence of the storage pulses which fail to store higher than first-rank coherences. These broadenings are largest with abundant nuclei with high gyromagnetic ratios (e.g. ^{27}Al, ^{11}B, ...). Baltisberger et al.[25] have shown that homonuclear broadenings will be a function of the

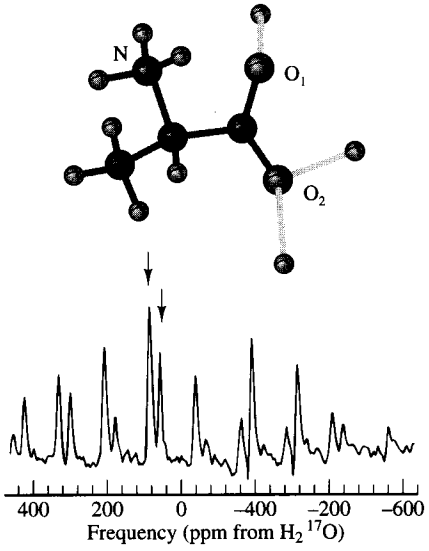

Figure 11 (Top) The structure of L-alanine showing the differences in hydrogen bonding on the two oxygen sites. (Bottom) Isotropic ^{17}O (0°,63.43°) CP DAS spectrum of L-alanine at 7.04 T with the two resolved centerbands for the two sites marked with arrows. (Adapted by permission of the International Society of Magnetic Resonance from S. L. Gann, et al.[28])

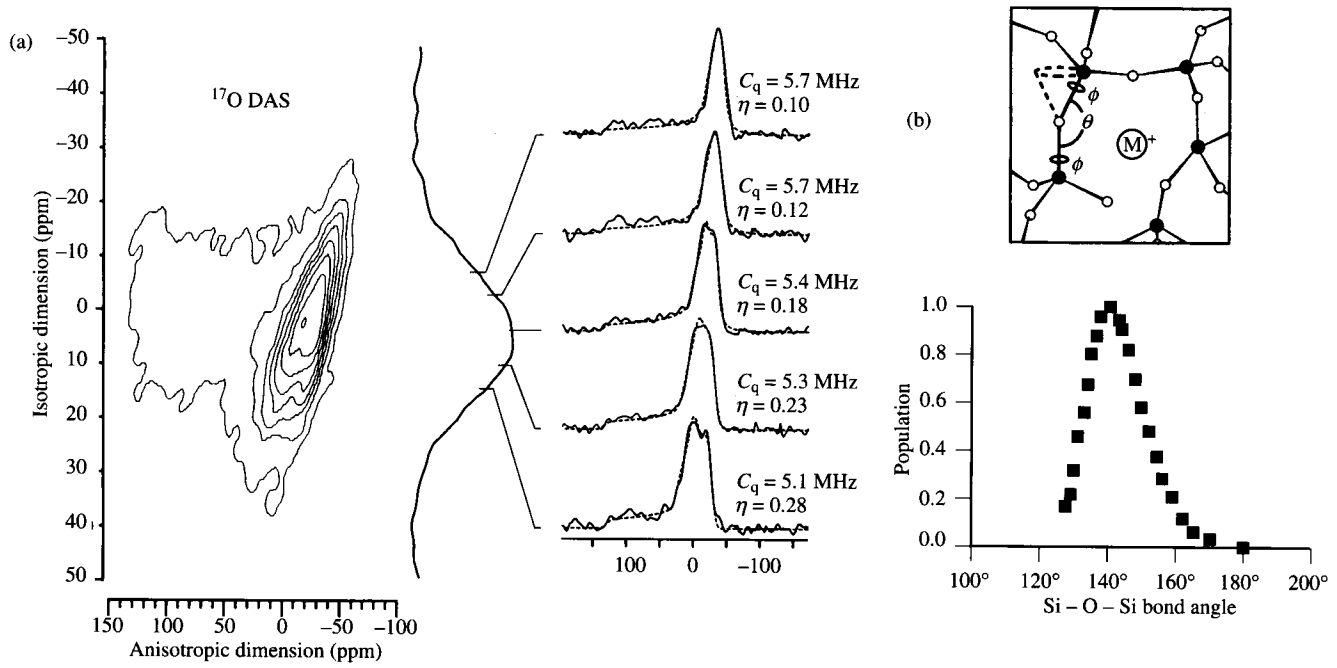

Figure 12 (a) ^{17}O 2D DAS spectrum of the bridging oxygen (Si–O–Si) resonances in $K_2Si_4O_9$ glass, shown together with the isotropic lineshape, and selected anisotropic cross sections correlated to specific frequencies in the isotropic lineshape. Because the glass contains a continuous distribution of Si–O–Si bond angles, and the ^{17}O isotropic frequency varies continuously with Si–O–Si bond angle, the bridging oxygen isotropic linewidth in the glass is ~ 25-times wider than a bridging oxygen resonance in a crystalline silicate. Since the ^{17}O anisotropic lineshapes for each Si–O–Si angle are separated in a 2D DAS spectrum, the separated anisotropic lineshapes can be fitted to obtain the isotropic lineshape as a function of the quadrupolar coupling parameters. With the help of experimental as well as ab initio based correlations between quadrupolar coupling parameters and the Si–O–Si bond angles, the isotropic lineshape can then be mapped into the Si–O–Si bond angle distribution for the glass. (b) The Si–O–Si bond angle distribution in $K_2Si_4O_9$ glass derived from its ^{17}O DAS spectra. (Adapted by permission of MacMillan Magazines Ltd. from Farnan, et al.[29])

DAS angle pair and the (0°,63.43°) angle pair produces spectra with the minimum broadenings; however, it does not eliminate it. For certain nuclei it is possible to eliminate the homonuclear dipolar broadenings using the isotopic depletion approach of Youngman and Zwanziger.[27] By enriching glassy B_2O_3 to 97% in ^{10}B, they obtained increased resolution by eliminating the ^{11}B dipolar broadenings from the ^{11}B DAS spectrum.

Another limitation arises from the finite time required to hop the rotor axis between the DAS angle pairs. When the spin–lattice relaxation time T_1 is on the order or less than the hop time ($T_1 \leqslant \tau_{hop}$) there will be significant losses in signal intensity. For this reason integrated intensities in DAS may not accurately reflect the site populations.

4 APPLICATIONS OF DAS

Since its development DAS has been successfully applied to a number of multisite crystalline compounds. Mueller and co-workers[14,15] have applied ^{17}O DAS to a number of crystalline silicates, resolving inequivalent bridging (Si–O–Si) and non-bridging (Si–O–M) oxygens. Baltisberger et al.[16] have applied ^{87}Rb DAS to a number of crystalline inorganic rubidium salts and obtained isotropic spectra along with correlated anisotropic spectra from which quadrupolar coupling parameters could be obtained. Gann et al.[28] obtained the spectrum shown in Figure 11 where they could resolve the two crystallographically distinct oxygen sites of L-alanine in a (0°,63.43°) CP DAS experiment.

Farnan et al.[29] showed that DAS is particularly advantageous when applied to amorphous samples (see also ***Amorphous Materials***) where a continuous structural distribution results in a continuous distribution of anisotropic lineshapes. In the 2D DAS spectrum these anisotropic lineshapes can be separated according to their isotropic frequencies, analyzed, and then used to help map the isotropic lineshape into structural distributions. Figure 12(a) depicts a 2D ^{17}O DAS spectrum of the bridging oxygen (Si–O–Si) resonances in $K_2Si_4O_9$ glass. In this case the Si–O–Si bond angle distribution in Figure 12(b) was derived from the 2D DAS spectrum.

5 RELATED ARTICLES

Amorphous Materials; Double Rotation; Line Narrowing Methods in Solids; Magic Angle Spinning; Magic Angle Turning & Hopping; Multidimensional Spectroscopy: Concepts; Quadrupolar Interactions; Quadrupolar Nuclei in Glasses; Quadrupolar Nuclei in Solids; Sideband Analysis in Magic Angle Spinning NMR of Solids; Variable Angle Sample Spinning.

For References see p. 1776

6 REFERENCES

1. S. Ganapathy, S. Schramm, and E. Oldfield, *J. Chem. Phys.*, 1982, **77**, 4360
2. A. Samoson, E. Lippmaa, and A. Pines, *Mol. Phys.*, 1988, **65**, 1013.
3. A. Llor and J. Virlet, *Chem. Phys. Lett.*, 1988, **152**, 248.
4. B. F. Chmelka, K. T. Mueller, A. Pines, J. Stebbins, Y. Wu, and J. W. Zwanziger, *Nature (London)*, 1989, **339**, 42.
5. K. T. Mueller, B. Q. Sun, G. C. Chingas, J. W. Zwanziger, T. Terao, and A. Pines, *J. Magn. Reson.*, 1990, **86**, 470.
6. T. Terao, T. Fujii, T. Onodera, and A. Saika, *Chem. Phys. Lett.*, 1984, **107**, 145.
7. A. Bax, N. M. Szeverenyi, and G. E. Maciel, *J. Magn. Reson.*, 1983, **55**, 494.
8. A. Bax, N. M. Szeverenyi, and G. E. Maciel, *J. Magn. Reson.*, 1983, **52**, 147.
9. M. Goldman, P. J. Grandinetti, A. Llor, Z. Olejniczak, J. R. Sachleben, and J. W. Zwanziger, *J. Chem. Phys.*, 1992, **97**, 8947.
10. A. Samoson, B. Q. Sun, and A. Pines, in 'Pulsed Magnetic Resonance: NMR, ESR, and Optics — A Recognition of E. L. Hahn', ed. D. M. S. Bagguley, Clarendon Press, Oxford, UK, 1992.
11. E. R. Andrew, A. Bradbury, and R. G. Eades, *Nature (London)*, 1958, **182**, 1659.
12. I. J. Lowe, *Phys. Rev. Lett.*, 1959, **2**, 285.
13. S. L. Gann, J. H. Baltisberger, and A. Pines, *Chem. Phys. Lett.*, 1993, **210**, 405.
14. K. T. Mueller, Y. Wu, B. F. Chmelka, J. Stebbins, and A. Pines, *J. Am. Chem. Soc.*, 1991, **113**, 32.
15. K. T. Mueller, J. H. Baltisberger, E. W. Wooten, and A. Pines, *J. Phys. Chem.*, 1992, **96**, 7001.
16. J. H. Baltisberger, S. L. Gann, E. W. Wooten, T. H. Chang, K. T. Mueller, and A. Pines, *J. Am. Chem. Soc.*, 1992, **114**, 7489.
17. M. A. Eastman, P. J. Grandinetti, Y. K. Lee, and A. Pines, *J. Magn. Reson.*, 1992, **98**, 333.
18. K. T. Mueller, E. W. Wooten, and A. Pines, *J. Magn. Reson.*, 1990, **92**, 620.
19. K. T. Mueller, G. C. Chingas, and A. Pines, *Rev. Sci. Instrum.*, 1991, **62**, 1445.
20. P. J. Grandinetti, J. H. Baltisberger, A. Llor, Y. K. Lee, U. Werner, M. A. Eastman, and A. Pines, *J. Magn. Reson., Ser. A*, 1993, **103**, 72.
21. P. J. Grandinetti, Y. K. Lee, J. H. Baltisberger, B. Q. Sun, and A. Pines, *J. Magn. Reson., Ser. A*, 1993, **102**, 195.
22. R. R. Ernst, G. Bodenhausen, and A. Wokaun, 'Principles of Nuclear Magnetic Resonance in One and Two Dimensions', Oxford University Press, Oxford, UK, 1987.
23. A. J. Vega, *J. Magn. Reson.*, 1992, **96**, 50.
24. A. J. Vega, *Solid State NMR*, 1992, **1**, 17.
25. J. H. Baltisberger, S. L. Gann, P. J. Grandinetti, and A. Pines, *Mol. Phys.*, 1994, **81**, 1109.
26. W. T. Dixon, *J. Chem. Phys.*, 1982, **77**, 1800.
27. R. E. Youngman and J. W. Zwanziger, *J. Non-Cryst. Solids*, 1994, **168**, 293.
28. S. L. Gann, J. H. Baltisberger, E. W. Wooten, H. Zimmerman, and A. Pines, *Bull. Magn. Reson.*, 1994, **16**, 68.
29. I. Farnan, P. J. Grandinetti, J. H. Baltisberger, J. F. Stebbins, U. Werner, M. A. Eastman, and A. Pines, *Nature (London)*, 1992, **358**, 31.

Biographical Sketch

Philip J. Grandinetti. *b* 1960. B.S., 1982, M.S., 1984, Chemistry, West Virginia University, USA (with Nar S. Dalal), Ph.D., 1988, Physical Chemistry, University of Illinois, USA (with Jiri Jonas). Postdoctoral fellow, 1989–93, University of California, Berkeley, USA (with Alex Pines). Faculty in Chemistry, Ohio State University, 1993–present. Approx. 20 publications. Current research interests: applications of solid state NMR to materials research.

For list of General Abbreviations see end-papers

Dynamic Frequency Shift

Lawrence G. Werbelow

Universite d'Aix-Marseille I, Marseille, France

1 INTRODUCTION

The proper treatment of a spin subject to two or more noncommuting interactions is a familar problem in nuclear magnetic resonance. In practice, various interactions usually differ markedly in magnitude, which enables one to choose the eigenfunctions of the dominant term as a zeroth-order approximation. (Throughout this discussion, the Zeeman interaction is considered dominant. Hence, the high-field approximation obtains). The effect of lesser interactions can be treated in the context of standard perturbation theory. A classic example is the case of a spin under the influence of a laboratory-fixed Zeeman interaction and a static, molecule-fixed quadrupole interaction. However, in certain situations, the first-order correction vanishes identically and it may be necessary to consider effects derived from higher-order perturbation theory. A well-known example is the treatment of the $\frac{1}{2} \leftrightarrow -\frac{1}{2}$ central transition of a half-integer spin subject to both Zeeman and quadrupolar interactions.

In contrast, when motions effectively average molecule-fixed interactions, first-order effects associated with quadrupole, dipole–dipole, or anisotropic electronic shieldings disappear completely in spherically symmetric or isotropic media. Nevertheless, if the averaging motions are slow on the timescale associated with reciprocal Larmor frequencies, a second-order shift of the Zeeman energy occurs even though first-order corrections are quenched.